Chapter 5

Spectroscopic and dielectric properties of crystallized $PbO-Sb_2O_3-As_2O_3$: NiO glass system

ABSTRACT

Glasses of the composition $40PbO-(20-x)Sb_2O_3-40As_2O_3$ were crystallized with different concentrations of NiO (x) ranging from 0 to 1.5 mol%. The samples were characterized by X-ray diffraction, scanning electron microscopy and differential thermal analysis techniques. The X-ray diffraction and the scanning electron microscopic studies have revealed the presence of $NiSb_2O_6$, $NiAs_2O_4$, $Ni_2As_2O_7$, $Pb_5Sb_2O_8$, $PbSb_2O_6$, $Pb_5Sb_4O_{11}$ crystalline phases in these samples. Spectroscopic (IR and optical absorption), magnetic and dielectric studies have been investigated. The IR spectral studies have pointed out the glass ceramic network is composed of conventional AsO_3 and SbO_3 structural units; these studies have further indicated that the decreasing concentration of symmetrical vibrations of above structural groups with increase in the concentration of NiO beyond 0.8 mol%. The analysis of the results of optical absorption, magnetic properties and dielectric properties have indicated that there is a gradual transformation of Ni^{2+} ions from octahedral to tetrahedral positions when the concentration of the crystallizing agent NiO is increased beyond 0.8 mol%. From these results it is also assessed that the glass crystallized with about 0.8 mol% of NiO is more suitable for getting maximum luminescence efficiency in the NIR region.

Spectroscopic and dielectric properties of crystallized $PbO\text{-}Sb_2O_3\text{-}As_2O_3$: NiO glass system

5.1 Introduction

Crystalline glass materials with appropriate transition metal ions like nickel as nucleating agents are considered as better candidates for ultra broad band optical amplifiers that are widely used in telecommunication systems [1]; in the glass ceramic materials non-radiative losses over the relaxation of excited states of luminescence ions is relatively low when compared with glasses and crystalline materials. Though, the rare earth ions doped glasses and glass ceramics were considered as the suitable candidates for such applications, but the optical amplification band width in these materials is narrowed, due to the fact that the emission bands of 4f – 4f transition of the rare earth ions are very sharp. Additionally, if the care is taken to minimize the size of the micro-crystals (far less than the wavelength of interest) in the glass ceramics during the synthesis, the light scattering caused by these crystals is negligibly low and thereby a substantial improvement in the quantum efficiency of the broad band emission can be achieved. Further, the lasing ions disperse more evenly in crystalline embryos of bulk glass ceramic samples when compared with amorphous samples.

Among various transition metal ions, Cr^{4+} ions were considered as potential candidates for high gain optical amplifiers with larger bandwidths in glass ceramics; nevertheless, the chromium ions exist in multi valence states, viz., Cr^{3+}, Cr^{4+}, Cr^{5+} and Cr^{6+} [2, 3]. The same is true in case of other transition metal ions like Ti, Mn etc. [4, 5]. Hence, it is too difficult to have the strict control over the required or suitable valence state of these ions embedded in crystal phases. Unlike these ions, the nickel ions mostly exist in divalent state and are extremely stable and no special care is necessary during synthesis to retain nickel ions in divalent state. There have been hardly any reports so far about reduction or oxidation of Ni^{2+} ions in to lower or higher oxidation states respectively in glasses or glass ceramic matrices during synthesis. Further, Ni^{2+} is an ion with exceptionally large crystal stabilization energies particularly when it is in octahedral field [6]. Ni^{2+} ions exhibit several strong absorption bands in the visible and NIR regions where the pumping sources are easily available. The octahedrally positioned Ni^{2+} ions in glass network are expected to exhibit eye safe laser emission of wavelength about 1.5 μm due to $^3T_2 \rightarrow {}^3A_2$ transition, even at room temperature, which is of great importance in telecommunications [7]. There have been considerable recent studies on lasing action and other physical properties of nickel ions in various glass and glass ceramic materials [8-11].

This part of the thesis is devoted to report a variety of physical properties that include dielectric studies, spectroscopic studies (IR, optical absorption) of crystallized $PbO\text{-}Sb_2O_3\text{-}As_2O_3$ glasses with varying concentrations of NiO as nucleant. The crystallization behavior and microstructure of glass ceramic products produced have also been investigated by means of XRD, SEM, DTA and EDS. The study is also intended to comment on the suitability of these glass ceramic materials for laser emission in NIR region.

5.2 Brief review of the previous work on glasses and glass ceramics containing nickel ions

Baiocchi et al [12] have studied optical and magnetic properties of nickel ions in lead silicate glasses; they have found that Ni^{2+} ions are both four fold and six fold coordinated in the glasses. They have assigned the bands observed in the optical absorption spectrum to the corresponding transitions on the basis of ligand field calculations. Paul and Tiwari [13] from their studies on Ni^{2+} ions in silicate glasses have concluded that Ni^{2+} can behave as network formers in the right conditions of temperature and composition. Yokokawa et al [14] have reported studies of NiO dissolved alkali silicate glasses based on redox potential and visible absorption spectra. From the studies they have concluded that the Ni^{2+} ions exist in tetrahedral and octahedral coordinations in these glasses. The studies also revealed that

the relative ratio of tetrahedral to octahedral species of Ni^{2+} depends on the concentration of NiO. Rao et al [15] have studied optical absorption spectra of Ni^{2+} ions in lead acetate glasses and interpreted the absorption bands in terms of ligand field theory.

Musinu and Piccaluga [16] have investigated the environment of nickel ions in alkali phosphate glasses by X-ray diffraction and determined the coordination of nickel ions. Corrias et al [17] have studied the structure of nickel phosphate glasses by neutron scattering with isotropic substitution for nickel. Kundu and Chakravorty [18] have investigated nickel the structural properties of titania glasses and concluded that the glass structure is built up by cross linking of NiO_3 triangular units with TiO_6 octahedron.

Singh and Singh [19] reported thermodynamic activity of nickel oxide in alkali silicate glasses and found that the activity coefficient of nickel oxide decreases with temperature. Kashif et al [20] have studied the structure and magnetic susceptibility of sodium borate glasses containing nickel oxide. Khalifa et al [21] have investigated the effect of duration of melting on the absorption spectra, molar volume and refractive index of nickel containing glasses. El-Desoky et al [22] have studied magnetic and electrical properties of lithium borosilicate glasses containing nickel oxide. Rajendran et al [23] have reported the propagation of ultrasonic waves in nickel doped calcium

aluminoborate glasses. Brendebach et al [24] investigated the effect of NiO dopant concentration in sodium metaphosphate glasses by means of X-ray absorption fine structure and UV/VIS/NIR spectroscopic investigations. Tawati and Adlan [25] have recently reported thermoelectric power of semiconducting cobalt phosphate glasses mixed with nickel oxide. These investigations have provided the information on the polaron formation and the disorder energy due to random fields in the glass matrix. Suzuki et al [26, 27] have studied the crystallization process and luminescence properties of lithium gallium silicate glass ceramics embedded with nickel nanocrystals. In these studies the luminescence emission observed at about 1300 nm was attributed to $^3T_{2g}$ (^3F) $\rightarrow$ $^3A_{2g}$ (^3F) transition of octahedral Ni site. Rao et al [28] reported the optical absorption and thermoluminescence properties of antimony borate glasses doped with NiO. The results were analyzed in the light of different environments of nickel ions. Schlenz et al [29] have carried out high energy X-ray diffraction studies on Ni doped sodium metaphosphate glasses. From these studies they have evaluated the average Ni-O distance as 2.03 A^o and the coordination of the nickel ion as in the glass network as 6.0.

In spite of these literature, still there is a lot of scope to investigate the role of nickel ions in the crystallization process and the influence on physical properties of $PbO\text{-}Sb_2O_3\text{-}As_2O_3$ glass system.

Within the possible glass forming region of $PbO\text{-}Sb_2O_3\text{-}As_2O_3$ system, a particular compositions $40PbO\text{-}(20\text{-}x)Sb_2O_3\text{-}40As_2O_3$: x NiO with the value of x ranging from 0 to 1.5 mol% is chosen for the present study; the samples are labeled as N_0 (x=0), N_2 (x=0.2), N_4 (x=0.4), N_6 (x=0.6), N_8 (x=0.8), N_{10} (x=1.0), N_{15} (x=1.5).

The glass specimens prepared with various concentrations of NiO were heat treated in a furnace at 300 ^oC for 6 h. Automatic controlling furnace was used to keep the temperature at the desired level. After the heat treatment in the furnace at specified temperature, the samples were chilled in air to room temperature. It may be noted here that as the concentration of NiO is increased, the colour of the glass ceramics is gradually turned from brown to thick brown and beyond 1.5 mol% of NiO, the colour of the samples became thick black and opaque. Hence, the concentration of the dopant is limited to only up to 1.5 mol%.

5. 3 Characterization

5.3.1 Scanning electron microscopy

The prepared $PbO\text{-}Sb_2O_3\text{-}As_2O_3$: NiO glass ceramic samples contain well defined, randomly distributed crystals entrenched in glassy matrix with an average diameter of 200-300 nm. The residual glass phase is acting as interconnecting zones among the crystallized areas making the samples free

of voids and cracks; this can be visualized clearly from the scanning microscopy pictures of the (Fig. 5.1) of samples. Thus, from these pictures it can also be concluded that NiO, enhanced the phase separation tendency of arious crystalline phases; this fact reflects specific overlap integral between the 3d levels of Ni ion and the delocalized anti-bonding p-states of antimony.

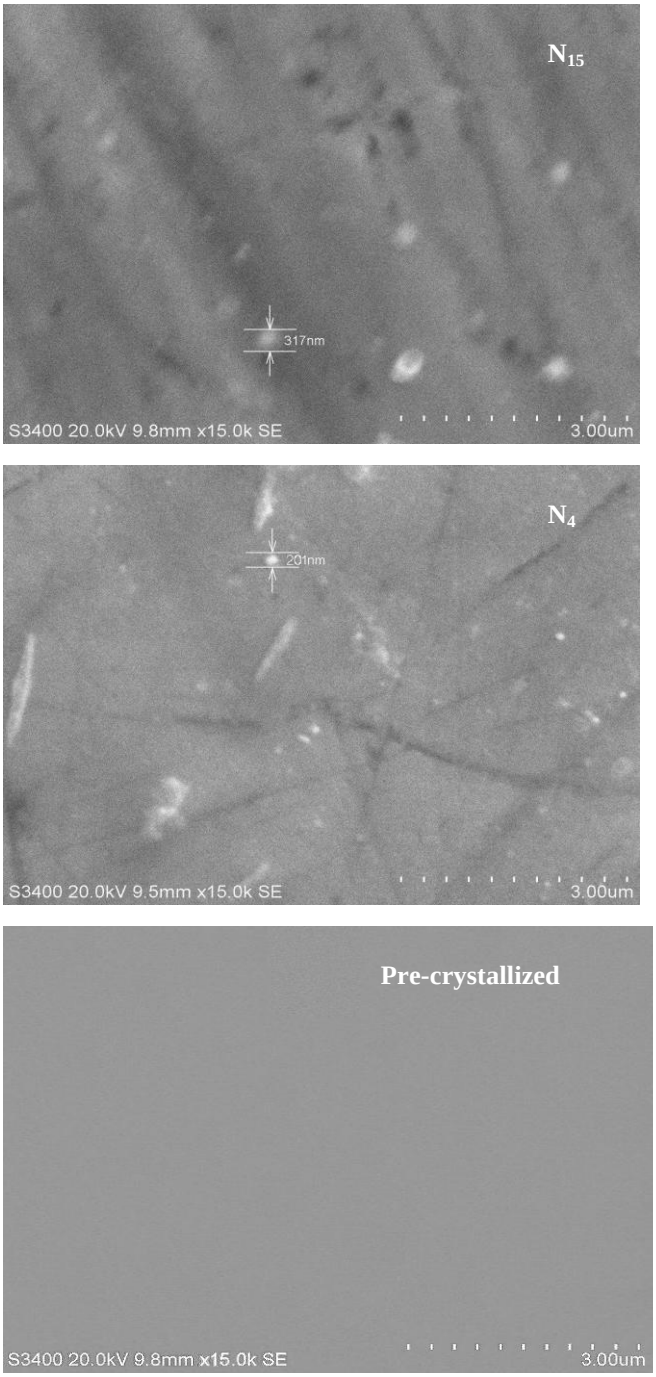

Fig. 5.1 SEM images for some of $PbO\text{-}Sb_2O_3\text{-}As_2O_3$: NiO glass ceramics doping with pre-crystallized glass

5.3.2 Energy dispersive spectra

The chemical makeup of the crystal phases is characterized using EDS (Fig. 5.2); the analysis indicated the presence of lead, arsenate, antimony, nickel and oxygen elements in the samples.

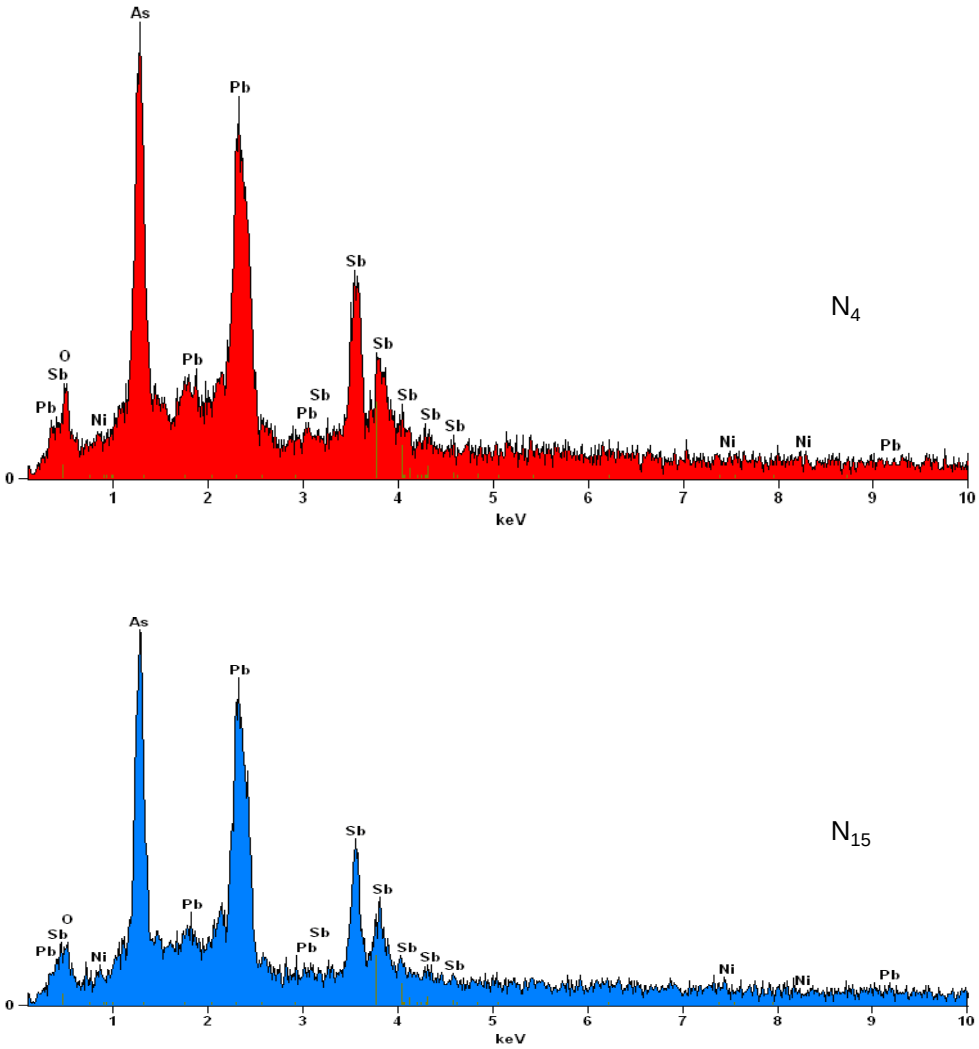

Fig. 5.2 EDS traces for some of the $PbO\text{-}Sb_2O_3\text{-}As_2O_3$: NiO glass ceramic samples.

1 $PbSb_2O_6$ 3 $NiSb_2O_6$ 5 $Pb_5Sb_4O_{11}$

2 $Ni_2As_2O_7$ 4 $NiAs_2O_4$ 6 $Pb_5Sb_2O_8$

5.3.3 X-ray diffraction studies

X-ray diffraction studies (Fig. 5.3) indicate the formation of $NiSb_2O_6$, $NiAs_2O_4$, $Ni_2As_2O_7$, $Pb_5Sb_2O_8$, $PbSb_2O_6$, $Pb_5Sb_4O_{11}$ (JCPDS card numbers

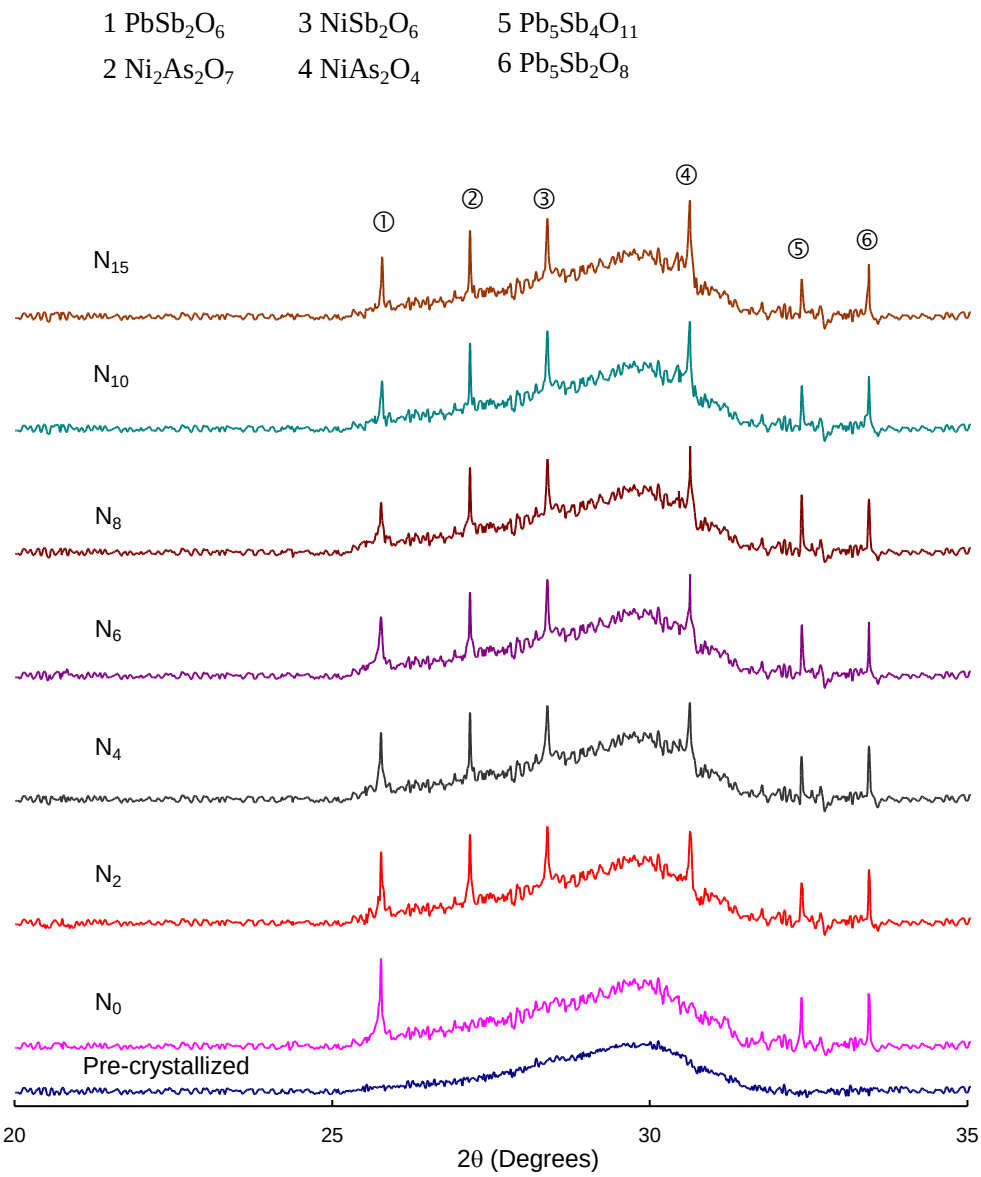

Fig. 5.3 XRD patterns of $PbO\text{-}Sb_2O_3\text{-}As_2O_3$ glasses crystallized with different concentrations of NiO.

38-1083, 44-0438, 10-0326, 22-0381, 34-0912 and 21-0941 respectively [30]) crystalline phases that are kinetically and thermodynamically feasible seemed to be products in these samples. The Ni rich areas in the samples may enhance the reactivity of Ni ion with the other oxides that precipitate as a high density of fine Ni rich crystals. These tiny crystals act as heterogeneous nuclei for the crystallization of the remaining glass. The diffraction data also indicate that, in these samples, the antimony ions exist in Sb^{5+} state in addition to Sb^{3+} state; however, the concentration of Sb^{3+} ions seems to be dominant over Sb^{5+} ions in the samples crystallized with lower concentrations of NiO.

5.3.4 Differential thermal analysis

In Fig. 5.4, we have shown differential thermal analysis traces (DTA) for some of the $PbO\text{-}Sb_2O_3\text{-}As_2O_3$: NiO glass ceramics in the temperature

Table 5.1

Summary of the data on differential thermal analysis

Glass	T_g (^oC)	T_c (^oC)	T_m (^oC)
N_2	242	378	568
N_4	244	377	572
N_6	247	378	576
N_8	249	365	584
N_{10}	260	392	590
N_{15}	271	405	603

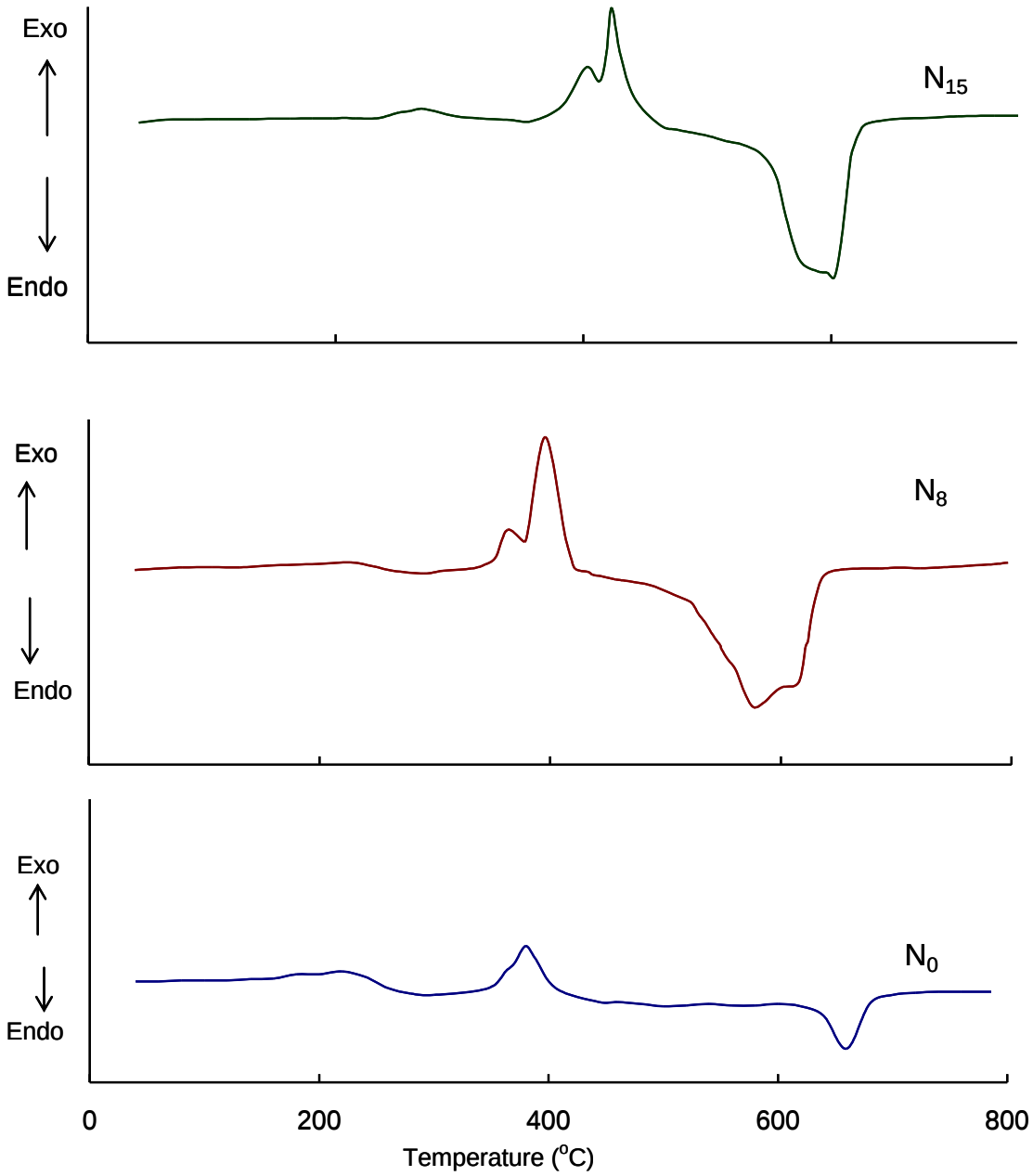

Fig. 5.4 Differential thermal analysis traces (DTA) for some of the PbO-Sb_2O_3-As_2O_3: NiO glass ceramics.

5.3.5 Physical parameters

The gradual increase of the content of nucleating agent NiO in the glass matrix, caused a slight increase in the density of these materials (Table 5.1). However, the values of density are always found to be higher than those of corresponding amorphous materials. From the measured values of the density and average molecular weight $\overline{M}$ of the samples, various other physical parameters such as nickel ion concentration N_i, mean nickel ion separation r_i, polaron radius r_p in $PbO\text{-}Sb_2O_3\text{-}As_2O_3$: NiO glass ceramic samples are computed and presented in Table 5.2.

Table 5.2

The physical properties of $PbO\text{-}Sb_2O_3\text{-}As_2O_3$: NiO glass ceramics (densities of pre-crystallized samples are shown in brackets).

Glass ceramic	N_0	N_2	N_4	N_6	N_8	N_{10}	N_{15}
Density d (gm/cm^3)	5.790 (5.735)	5.757 (5.738)	5.752 (5.741)	5.747 (5.744)	5.740 (5.737)	5.743 (5.740)	5.764 (5.757)
Average molecular weight $\overline{M}$	226.716	226.282	225.848	225.415	224.981	224.547	223.463
Ni^{2+} ion concent N_i (10^{22} ions/cm^3)	-	0.306	0.614	0.921	1.227	1.541	2.330
Inter ionic distance of Nickel ions r_i (A^o)	-	6.88	5.46	4.77	4.34	4.02	3.50
Polaron radius r_p (A^o)	-	2.77	2.20	1.92	1.75	1.62	1.41

5.4 Results

5.4.1 Optical absorption spectra

The optical absorption edge observed at 380 nm for glass N_2 is found to be shifted to higher wavelength with increase in the concentration of NiO up to 0.8 mol %; beyond this concentration the edge is observed to shift towards lower wavelength (Fig. 5.5). From the observed absorption edges, we have evaluated the optical band gaps (E_o) of these samples by drawing Urbach plots (Fig. 5.6) between $(\alpha\hbar\omega)^{1/2}$ and $\hbar\omega$. The value of the optical band gap exhibited a decreasing trend up to 0.8 mol% of NiO and beyond that is found to increase.

Additionally, the spectrum of the sample (N_2) exhibited, four clearly resolved absorption bands in the visible and NIR regions at 1274 nm (O_h1), 792 nm (O_h2) and 471 nm (O_h3) and 595 nm (tetrahedral band). As the concentration of NiO is increased up to 0.8 mol %, the intensity of the octahedral bands (O_h bands) is observed to increase with a shift towards slightly higher wavelength; in this concentration range the intensity of the tetrahedral band (T_d band) is observed to decrease with a slight shift towards higher wavelengths. With the raise of NiO content from 0.8 to 1.5 mol %, the tetrahedral band is observed to grow at the expense of octahedral

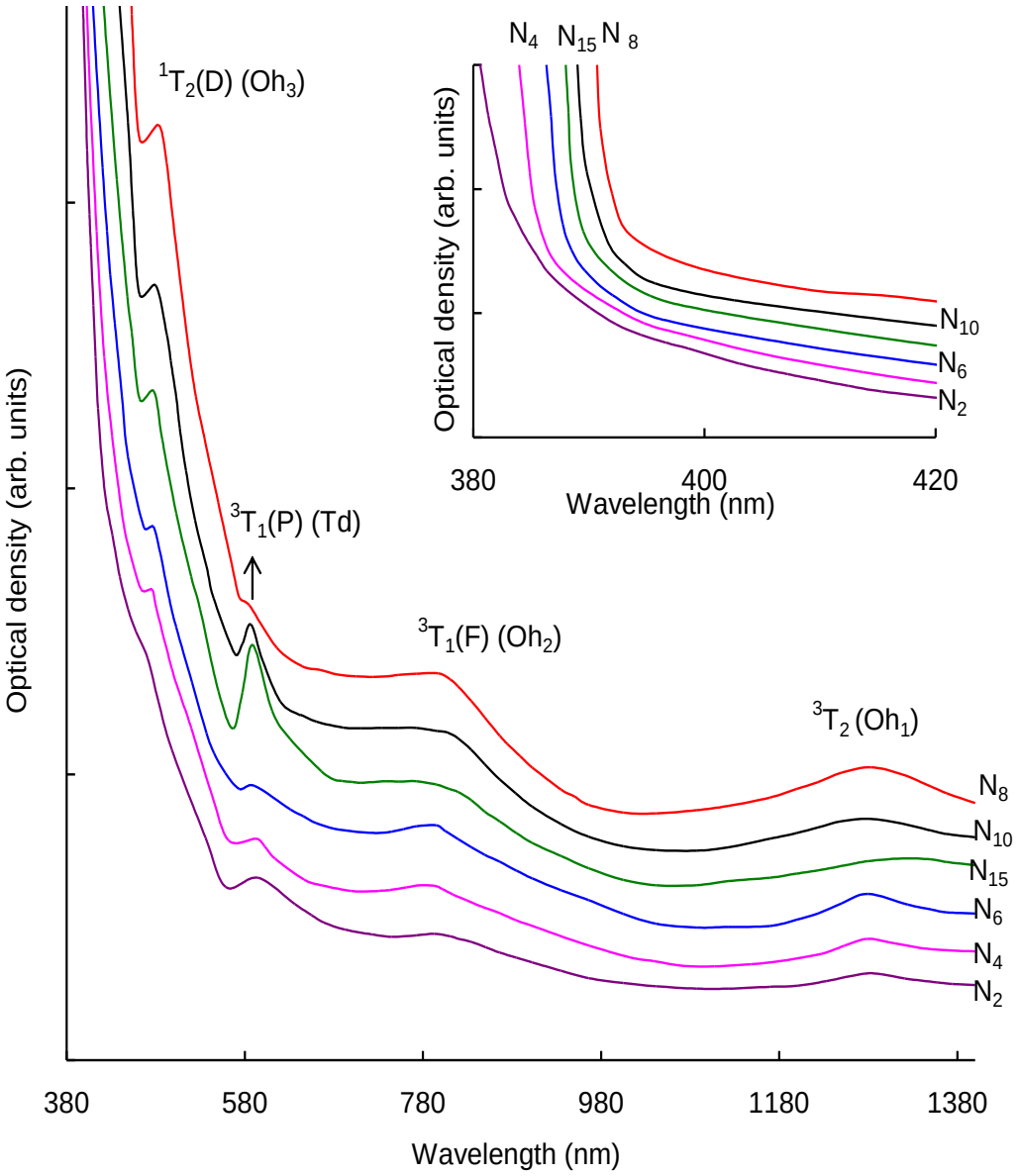

Fig. 5.5 Optical absorption spectra of $PbO\text{-}Sb_2O_3\text{-}As_2O_3$: NiO glass ceramics. Inset represents the absorption near the cutoff wavelength.

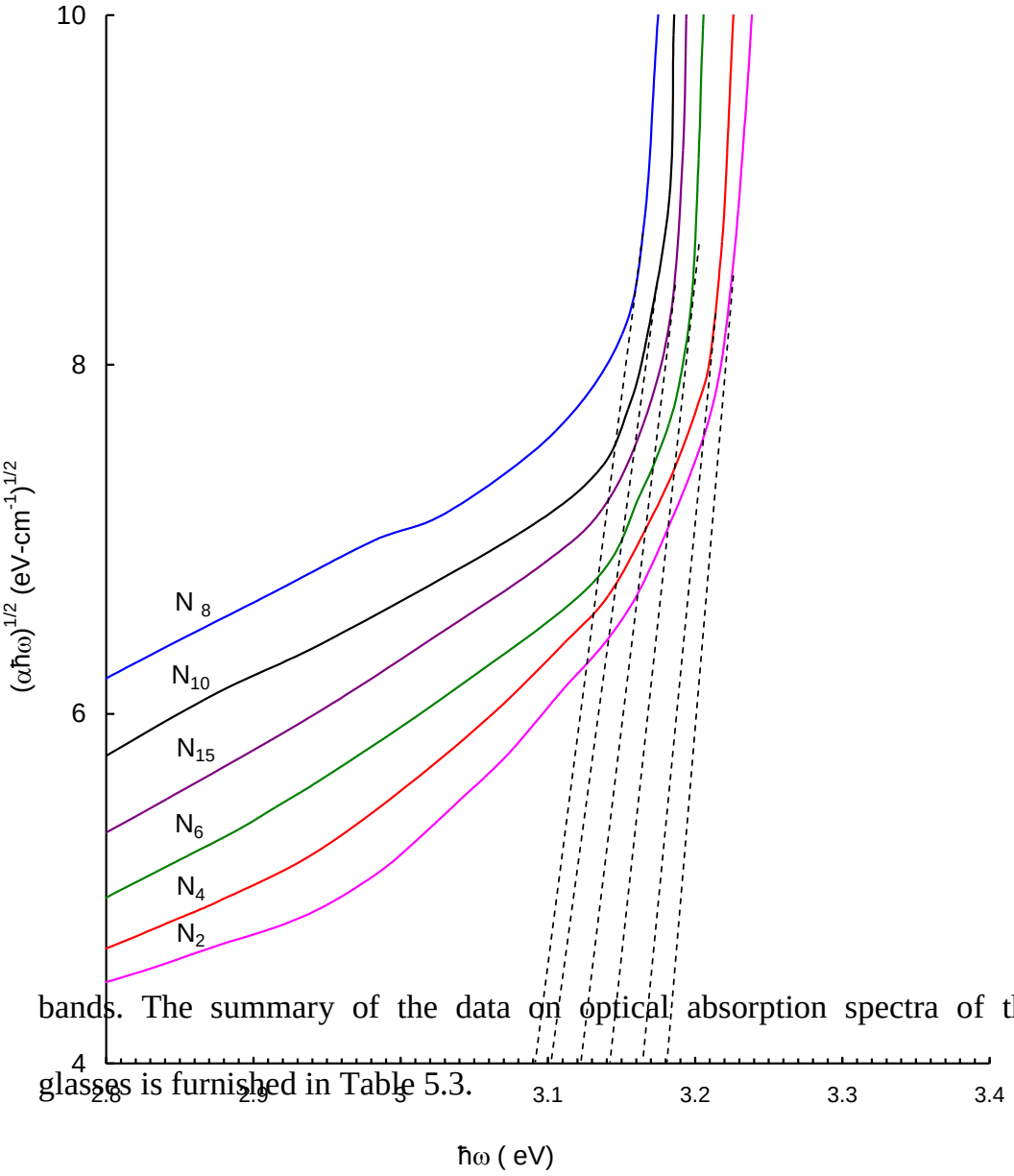

bands. The summary of the data on optical absorption spectra of these glasses is furnished in Table 5.3.

Fig. 5.6 Plots to evaluate optical band gaps for $PbO\text{-}Sb_2O_3\text{-}As_2O_3$: NiO glass ceramics.

Table 5.3

Summary of data on optical absorption spectra of $PbO\text{-}Sb_2O_3\text{-}As_2O_3$: NiO glass ceramics.

Transition of nickel ions	Band positions in nm					
	N_2	N_4	N_6	N_8	N_{10}	N_{15}
Octahedral transitions (nm)						
$^3A_2(F) \rightarrow {}^3T_2(F)$	1274	1278	1279	1283	1281	1280
$^3A_2(F) \rightarrow {}^3T_1(F)$	792	793	794	797	796	795
$^3A_2(F) \rightarrow {}^1T_2(D)$	471	476	477	483	480	478
Tetrahedral transitions (nm)						
$^3A_2(F) \rightarrow {}^3T_1(P)$	595	593	591	585	587	589
Cutoff wavelength (nm)	380	384	386	391	389	387
Optical band gap E_o (eV)	3.18	3.165	3.14	3.09	3.10	3.12
Dq (cm^{-1})	784.9	782.5	781.9	779.4	780.6	781.3
B (cm^{-1})	733.0	735.2	743.2	750.8	738.0	732.3
Nephelauxetic ratio	0.681	0.683	0.690	0.697	0.685	0.680

5.4.2 Magnetic susceptibility

Magnetic susceptibility of $PbO\text{-}Sb_2O_3\text{-}As_2O_3$: NiO glass ceramics measured at room temperature is observed to increase gradually with increase in the content of crystallizing agent NiO. From the values of magnetic susceptibilities, the magnetic moment of Ni^{2+} ion is evaluated and presented in Table 5.4.

Table 5.4
Summary of data on magnetic properties of $PbO\text{-}Sb_2O_3\text{-}As_2O_3$: NiO glass ceramics.

Glass ceramic	Conc. NiO (mol %)	Magnetic susceptibility χ (10^{-5} emu)	μ_{eff} (μ_B)
N_2	0.2	1.89	3.00
N_4	0.4	4.04	3.10
N_6	0.6	6.63	3.24
N_8	0.8	9.27	3.33
N_{10}	1.0	16.1	3.90
N_{15}	1.5	26.2	4.05

5.4.3 ***Infrared spectra***

In the infrared spectrum (Fig. 5.7) of glass ceramic sample N_2, the band due to ν_1 vibrations of SbO_3 structural groups is observed at about 943 cm^{-1} and the band related to ν_2 vibrations of these units is observed at 621 cm^{-1}. The IR spectrum of crystalline As_2O_3 is expected to exhibit four fundamental absorption bands at ν_1 (1050 cm^{-1}), ν_2 (618 cm^{-1}), ν_3 (795 cm^{-1}) and ν_4 (505 cm^{-1}) [31]. In the spectrum of glass ceramic N_2, the ν_1 band is

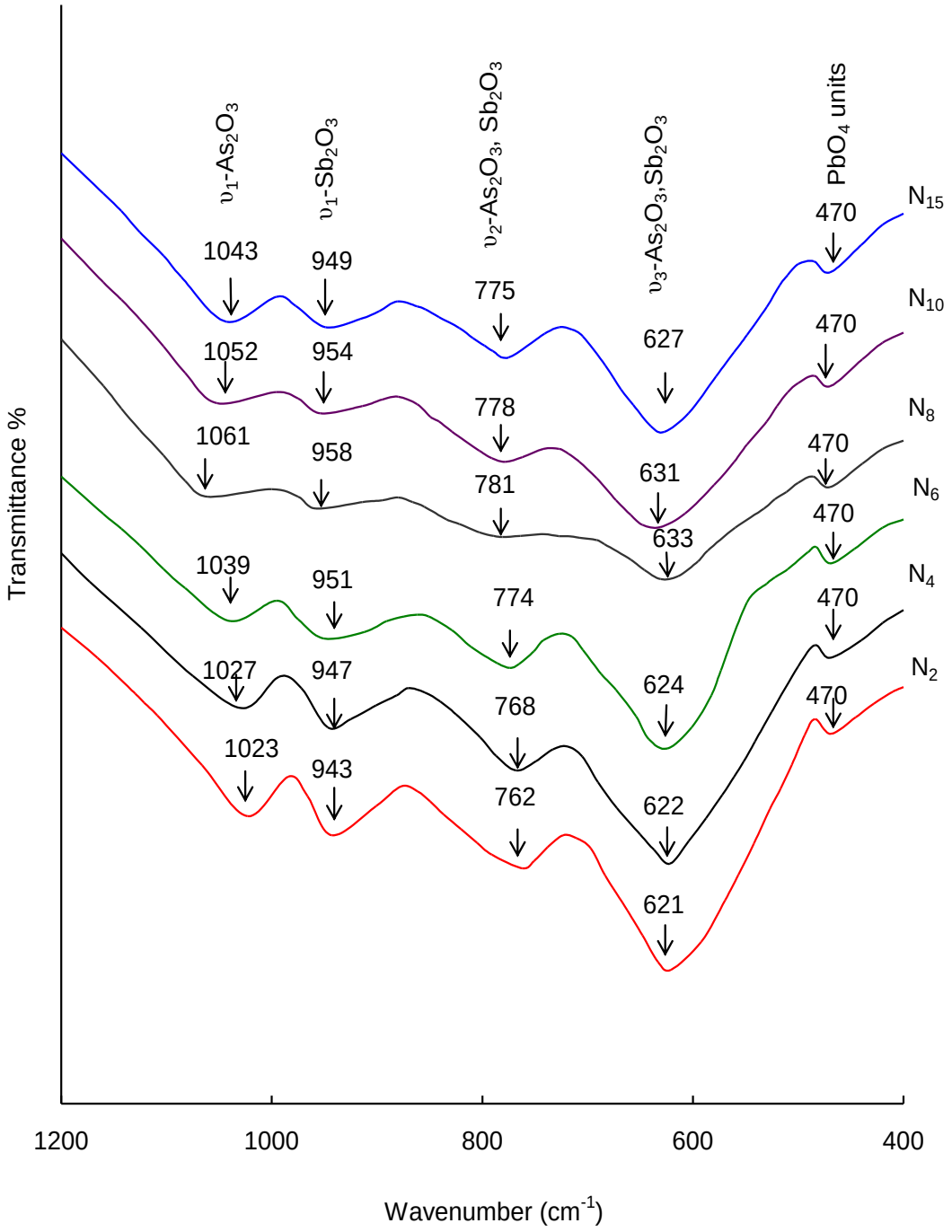

Fig. 5.7 IR spectra of $PbO\text{-}Sb_2O_3\text{-}As_2O_3$:NiO glass ceramics.

appeared at 1040 cm^{-1}, where as, the ν_2 bands and the ν_3 bands of SbO_3 and AsO_3 structural groups are merged and exhibited common meta-centres at 621 and 762 cm^{-1}, respectively. In the region of ν_4 vibrations of AsO_3 structural units, it is quite likely that the vibrations due to PbO_4 structural groups could be present; in fact the vibrational band due to PbO_4 units was reported at 470 cm^{-1} in a number of other glass systems [32]. The summary of IR spectra of these samples is shown Table 5.5. As the content of the crystallizing agent

Table 5.5
Summary of the data on the positions of the bands in IR spectra of PbO-Sb_2O_3-As_2O_3: NiO glass ceramics

Glass ceramic	ν_1 (cm^{-1})		As_2O_3 / Sb_2O_3 (cm^{-1})		PbO_4 (cm^{-1})
	As_2O_3	Sb_2O_3	ν_3	ν_2	
N_2	1023	943	621	762	470
N_4	1027	947	622	768	470
N_6	1039	951	624	774	470
N_8	1061	958	633	781	470
N_{10}	1052	954	631	778	470
N_{15}	1043	949	627	775	470

NiO is increased gradually up to 0.8 mol%, the intensity of bands due to symmetric stretching and symmetric bending vibrations of SbO_3 and AsO_3 structural groups is also observed to decrease; for further increase of NiO content these bands have exhibited a reversal trend.

5.4.4 Dielectric properties

The dielectric constant ε' and loss tan δ at room temperature (≈ 30 ^{o}C) of PbO-Sb_2O_3-As_2O_3 glass crystallized with 0.2 mol% of NiO at 100 kHz are measured to be 11.5 and 0.011 respectively; these values are found to increase considerably with decrease in frequency. Fig. 5.8 represents the variation of dielectric constant and loss with frequency at room temperature of PbO-Sb_2O_3-As_2O_3 glasses crystallized with different concentrations of NiO; the parameters, ε' and tanδ are observed to increase with the concentration of NiO up to 0.8 mol% at any frequency.

The temperature dependence of ε' at 1 kHz of PbO-Sb_2O_3-As_2O_3 glasses crystallized with different concentrations of NiO is shown in Fig. 5.9 and at different frequencies of glass ceramic sample N_8 is shown as the inset. The value of $\varepsilon^{'}$ is found to exhibit a considerable increase at higher temperatures especially at lower frequencies; however the rate of increase of $\varepsilon^{'}$ with temperature is found to be the maximum for the samples N_8.

A comparison plot of variation of tan δ with temperature, measured at a frequency of 10 kHz for all the glass ceramic samples is presented in Fig. 5.10. The inset (a) of this figure represents the temperature dependence of

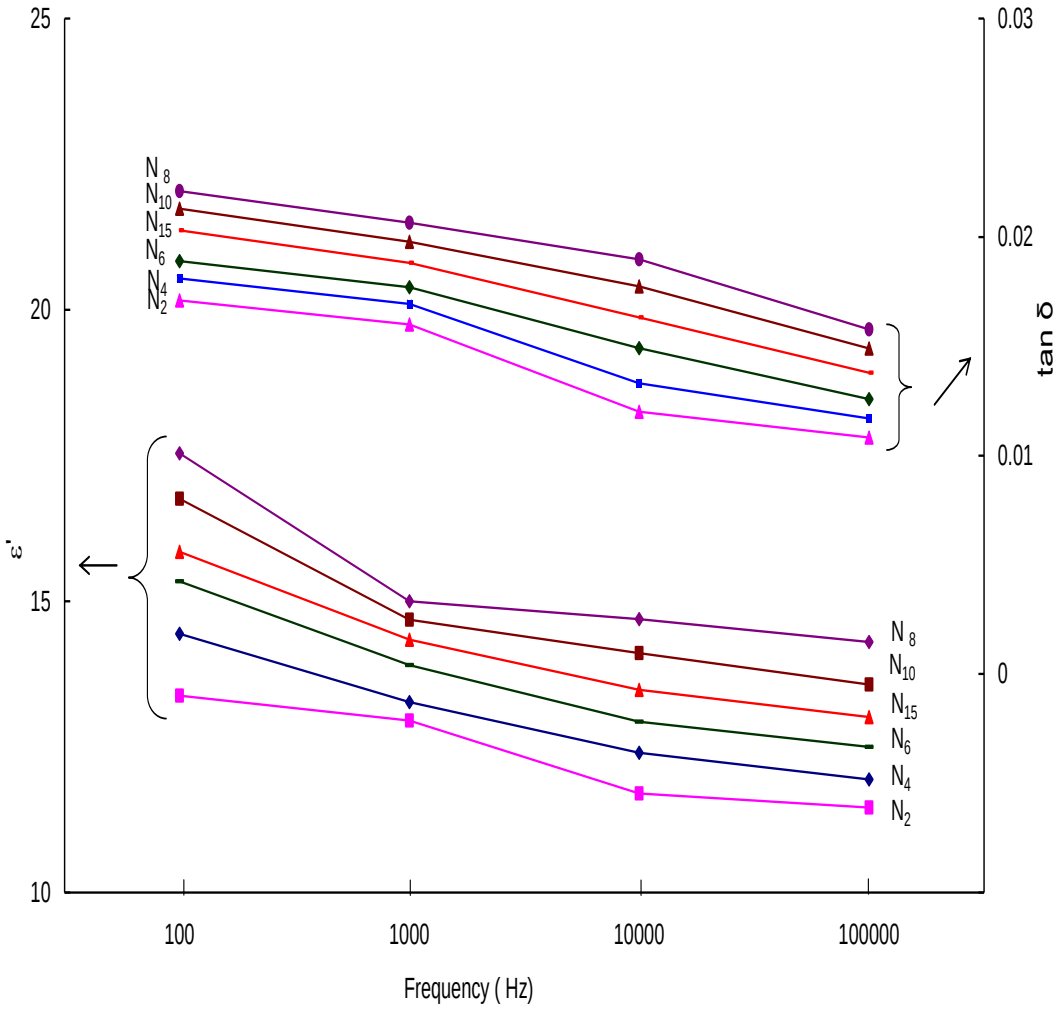

Fig. 5.8 Variation of dielectric constant and loss with frequency of PbO-Sb_2O_3-As_2O_3: NiO samples measured at room temperature

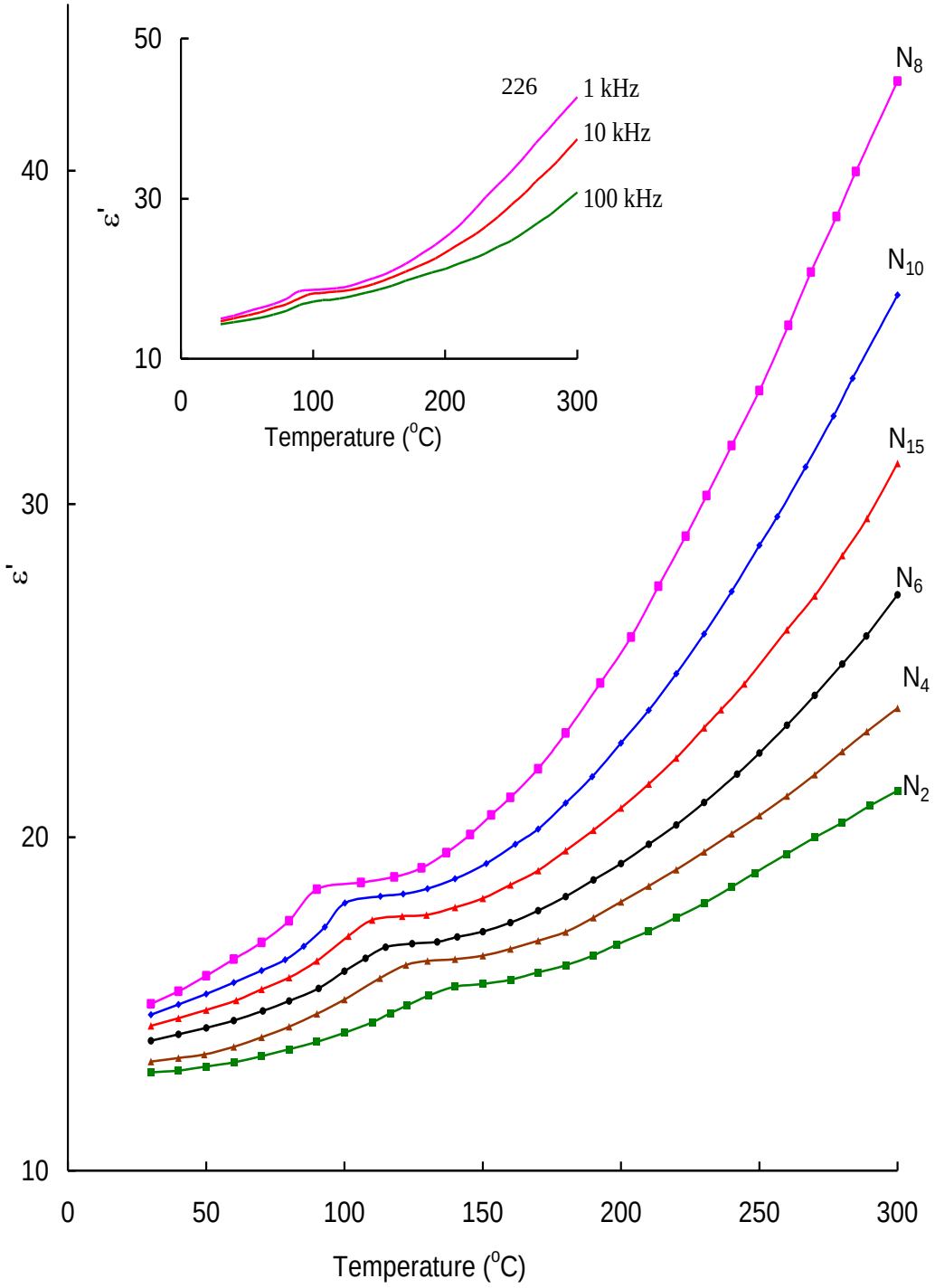

Fig. 5.9 A comparison plot of variation of dielectric constant with temperature at 1 kHz for $PbO\text{-}Sb_2O_3\text{-}As_2O_3$: NiO glass ceramics. Inset gives the variation of dielectric constant with temperature at different frequencies of glass ceramic N_8.

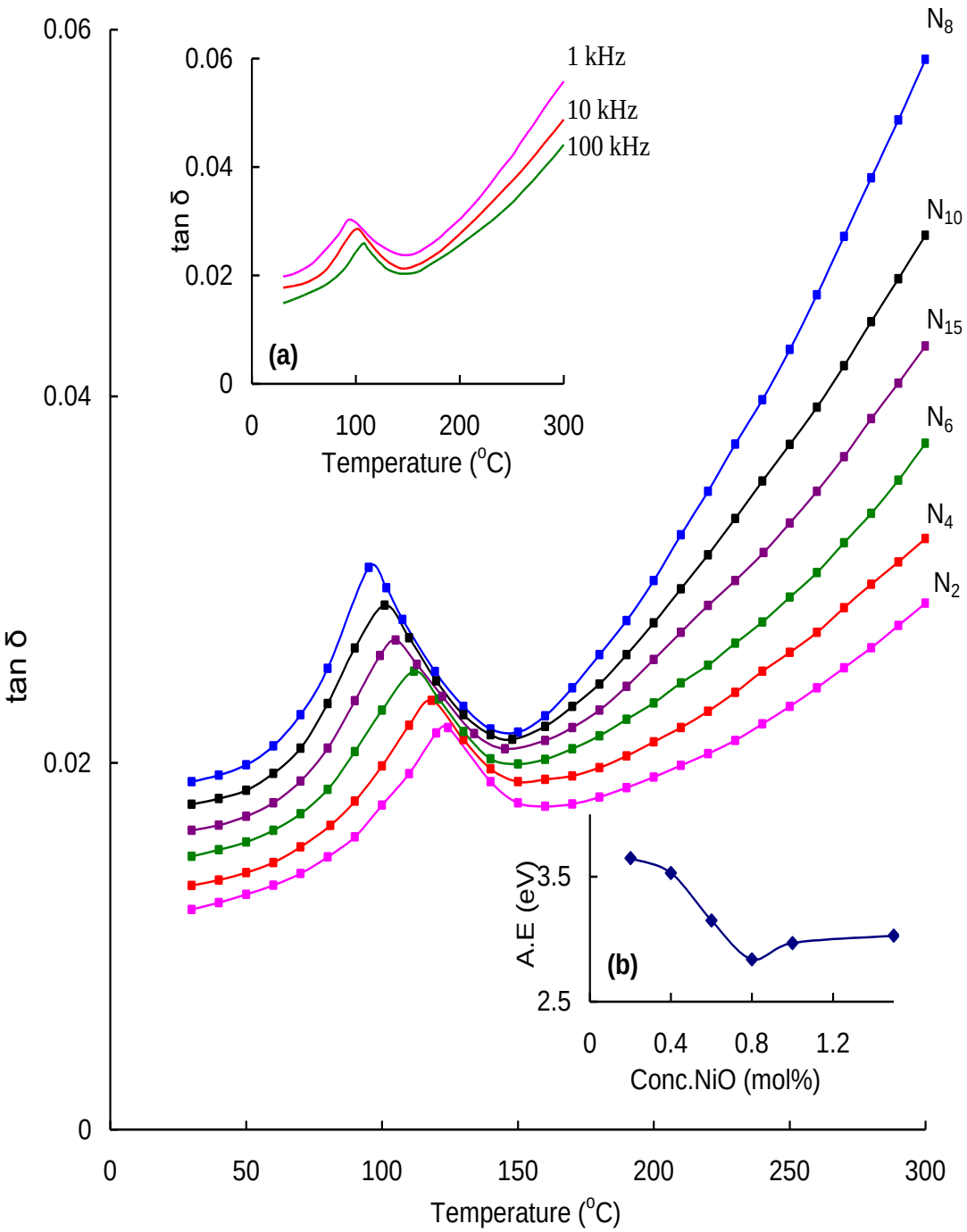

Fig. 5.10 A comparison plot of variation of dielectric loss with temperature at 10 kHz for PbO-Sb_2O_3-As_2O_3: NiO glass ceramics. Inset (a) gives the variation of dielectric loss with temperature at different frequencies of glass ceramic N_{10} and inset (b) shows the variation of activation energy for dipoles with the concentration of nucleating agent.

tan δ of sample N_{10} at different frequencies. The dependence of dielectric loss with temperature at different frequencies exhibits distinct maxima indicating dipolar relaxation character of dielectric loss in these glass ceramic samples. From these curves, it is also observed that the region of relaxation shifts towards lower temperatures (with broadening of relaxation peaks and increasing value of $(\tan \delta)_{max}$ with increase in the concentration of the nucleating agent up to 0.8 mol%. The effective activation energy W_d for the dipoles is evaluated for all the glass ceramic samples and its variation with the concentration of NiO is shown as inset (b) of Fig. 5.10; the activation energy is found to be minimum for the sample N_8. The pertinent data related to dielectric loss of these glasses is presented in Table 5.6.

Table 5.6

Data on dielectric loss of $PbO\text{-}Sb_2O_3\text{-}As_2O_3$: NiO glass ceramics.

Glass ceramic	$(\text{Tan } \delta)_{Max.Avg}$	Temp. region of relaxation(^oC)	A.E. for dipoles (eV)
N_2	0.0222	100-140	3.65
N_4	0.0236	90-132	3.53
N_6	0.0251	85-128	3.15
N_8	0.0300	70-115	2.84
N_{10}	0.0282	76-112	2.97
N_{15}	0.0268	80-115	3.03

The a.c. conductivity σ_{ac} is calculated at different temperatures for different frequencies and the plots of log σ_{ac} against 1/T are shown in Fig. 5.11 for all the glass ceramics at 100 kHz. From these plots, the activation energy for conduction in the high temperature region over which a near linear dependence of log σ_{ac} with 1/T could be observed is evaluated and presented in Table 5.7; this activation energy is also found to decrease gradually with increase in the concentration of the crystallizing agent up to 0.8 mol% (inset (a) of Fig. 5.11).

Table 5.7

Summary of data on ac conductivity of PbO-Sb_2O_3-As_2O_3: NiO glass ceramics.

Glass ceramic	$N(E_F)$ in (10^{20}, eV^{-1}/cm^3)	A.E. for conduction (eV)
N_2	1.960	0.36
N_4	2.105	0.33
N_6	2.288	0.30
N_8	2.778	0.23
N_{10}	2.622	0.26
N_{15}	2.452	0.28

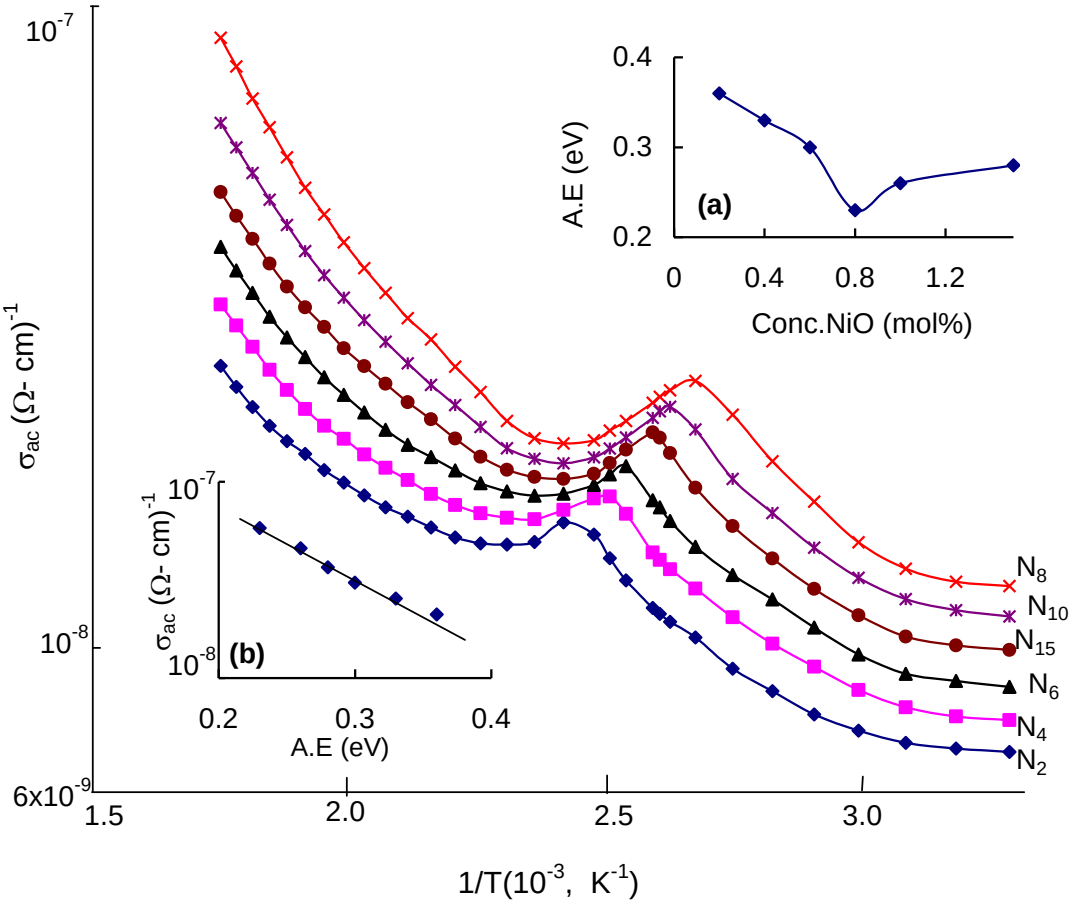

Fig. 5.11 Variation of σ_{ac} with 1/T at 100 kHz of $PbO\text{-}Sb_2O_3\text{-}As_2O_3$: NiO glass ceramic. Inset (a) represents the variation of activation energy for conduction with NiO concentration. Inset (b) shows the variation of log σ□(ω) vs. activation energy for conduction.

5.5 Discussion

In $PbO\text{-}Sb_2O_3\text{-}As_2O_3$: NiO glass system, Sb_2O_3 is an incipient glass network former and as such does not readily form the glass but does so in the presence of the modifier oxides like PbO and the strong glass former As_2O_3. Antimony oxide participates in the glass network with SbO_3 structural units with the oxygen at three corners and the lone pair of electrons of antimony at the fourth corner as mentioned earlier. In the glass network, normally the Sb-O distances lie in between 2.0 and 2.6 A° [33-35]. The coordination polyhedra are joined by sharing the corners to form double infinite chains with the lone pairs pointing out from the chains. X-ray diffraction studies have indicated that antimony ions also exist in Sb^{5+} state in these glass ceramics. As a participant of glass network, the local structure of Sb^{3+} cations become less symmetric and the strain energy in the glass network increases as a whole, thus resulting in a decrease in the additional activation energy that is necessary for glass network rearrangement. As a result we expect that more degree of disorder in glass ceramics containing Sb^{3+} ions rather than in the glass ceramics containing Sb^{5+} ions. Sb^{5+} ion participate in the glass network with $Sb^{V}O_4$ structural units as reported earlier [36].

As_2O_3 is a strong network former with corner sharing AsO_3 pyramidal units [37, 38]. Further, there is a possibility for the cross linking of a part of

SbO_3 units with As^{3+} ions to form Sb-O-As bonds in the glass network. The presence of common meta centers units of ν_2 and ν_3 vibrational bands in the ranges of SbO_3 and AsO_3 structural units, in the IR spectra of the glass ceramics in fact supports such a view point. However, earlier EXAFS studies indicated that $Sb^{V}O_4$ units are more compatible in the network forming rather than SbO_3 trigonal pyramids units to form linkages with the conventional AsO_3 structural units [39]. The reasons are obvious; Sb^{3+} ion with its lone electron pair occupies a greater angular volume than a bonding pair of electrons. As a participant of glass network, the local structure of Sb^{3+} cations become less symmetric and the strain energy in the glass network increases as a whole, thus resulting in a decrease in the additional activation energy that is necessary for glass network rearrangement. As a result we expect that more degree of disorder in glasses containing Sb^{3+} ions rather than in the glasses containing Sb^{5+} ions.

In general, the degree of structural compactness, the modification of the geometrical configuration of the glassy network, the size of the micro-crystals formed, change in the coordination of the glass forming ions and the fluctuations in the dimensions of the interstitial holes are the some of the factors that influence the density of the glass ceramic material. In the present case, progressive introduction of crystallizing agent NiO up to 0.8 mol%

caused a considerable decrease in the density; this is an indicative of decreasing structural compactness of the material. The higher values of density observed for the sample N_{15} indicates higher compactness for this sample.

The formation of $NiSb_2O_6$, $NiAs_2O_4$, $Ni_2As_2O_7$, $Pb_5Sb_2O_{8,}$ $PbSb_2O_6$, $Pb_5Sb_4O_{11}$ crystalline phases detected from the XRD studies indicate the presence of $NiSb_2O_6$, $PbSb_2O_6$ phases clearly confirms the conversion of a fraction of Sb^{3+} ions in to Sb^{5+} state in these glass ceramics.. The relative variation in the intensity of the diffraction patterns also indicates the presence of higher concentration Sb^{5+} in the samples N_{10} and N_{15}. The presence of different crystalline phases in these samples can also be visualized from scanning electron microscope pictures. The residual glass phase may act as interconnecting zones among the crystallized areas making the samples free of voids and cracks.

The appearance of different crystallization temperatures in the differential thermal analysis patterns of the glass ceramic samples obviously suggests the presence of different phases of crystallization in the samples. The analysis of the results of DTA studies indicates that with increase in the concentration of crystallizing agent NiO (beyond 0.8 mol%), there is a considerable increase in the glass transition temperature T_g. The higher

augmented cross-link density of various structural groups and the increment in the closeness of packing are responsible for such increase of this parameter. These results apparently suggest that there is a growing presence of tetrahedrally positioned nickel ions which increase the cross-link density and decrease the mean bond strength. The appearance of different crystallization temperatures in the DTA pattern obviously suggests the presence of different phases of crystallization in the samples. The low degree of resolution of exothermic peaks of the samples indicates overlapping of these peaks due to different crystalline phases.

The general shape of the crystallization peaks is strongly dependent with the nature of crystallization (bulk or surface) in the sample. For the surface crystallization we expect relatively wider peaks when compared with the peaks due to bulk crystallization [40]. The close examination of pattern of the DTA peaks reveals the enthalpy associated with the crystallization effect relatively small for the samples N_{10} and N_{15} indicating bulk crystallization prevails in these samples when compared with the rest of the samples.

Using Tanabe-Sugano diagrams for d^8 ion, the observed octahedral bands in the optical absorption spectra are assigned to $^3A_2$ (F) $\rightarrow$ $^3T_2$ (F) (Oh_1), $^3T_1$ (F) (Oh_2), $^1T_2$ (D) (Oh_3). Out of these, $^3A_2$ (F) $\rightarrow$ $^1T_2$ (D) is

attributed to spin forbidden octahedral band [41]. The band observed at about 595 nm is attributed to $^3A_2$ (F) $\rightarrow$ $^3T_1$ (P) tetrahedral transition [42]. The ligand field parameters Dq (crystal field splitting energy) and B (Racah parameter) are evaluated using energies of these transitions and the values obtained are furnished in Table 3. The observed enhancement of the absorption in the octahedral bands with increase in the content of NiO up to 0.8 mol% suggests the increasing presence of octahedrally positioned nickel ions and the increasing trend of tetrahedral band beyond 0.8 mol% of NiO indicates that the nickel ions prefer tetrahedral positions in this concentration range.

Further, the nephelauxetic ratio (β) evaluated from the Racah parameter (B), shows a decreasing trend; such a trend clearly suggests the decrease of the covalency around Ni^{2+} as the concentration of the nucleating agent is increased up to 0.8 mol%. The increasing trend of these values beyond 0.8 mol% of nucleating agent, indicates the increasing covalency environment for Ni^{2+} ions in the glass ceramic network. In the spectra, we have also observed the shifting of the octahedral bands towards higher wavelengths as the concentration of NiO is increased up to 0.8 mol%; such shift in the position of the bands indicates an increase in average distance of Ni-O.

The observed decrease in the optical band gap with the increase in the concentration of the nucleating agent may be understood as follows: the gradual increase in the concentration of octahedrally positioned Ni^{2+} ions, causes a creation of large number of donor centers; subsequently, the excited states of localized electrons originally trapped on Ni^{2+} sites begin to overlap with the unfilled 3d states on the neighboring impurity sites. As a result, the impurity band becomes more extended into the main band gap. This development might have shifted the absorption edge to the lower energy (Table 3) which leads up to a significant shrinkage in the band gap from the sample N_2 to N_8.

The magnetic properties of $PbO\text{-}Sb_2O_3\text{-}As_2O_3$: NiO glass ceramic samples arise from the paramagnetic Ni^{2+} (both tetrahedral and octahedral) ions. Magnetically, the octahedral Ni^{2+} complexes have relatively simple behaviour and their magnetic moments are expected to lie in the range 2.9 to 3.4 μ_B [43] depending on the magnitude of the orbital contribution. Since, the ground state $^3T_1$ (F) of tetrahedral Ni^{2+} ions possess much inherent orbital angular momentum, the magnetic moment of perfect tetrahedral Ni^{2+} should be ~ 4.2 μ_B. Even a slight distortion reduces this value markedly because of the orbital degeneracy. The fairly regular tetrahedral complexes of these ions are expected to have the magnetic moment in the range 3.5 to 4.1 μ_B [43]. The gradual increase of the effective

magnetic moment from 3.33 μ_B (for sample N_8) to 4.05 μ_B (for sample N_{15}) confirms that there is a gradual transformation of the positions of Ni^{2+} ions from the octahedral sites to the tetrahedral sites as the concentration of crystallizing agent NiO is increased beyond 0.8 mol %.

The decrease in the intensity of the bands due to symmetric stretching and bending vibrations of AsO_3 and SbO_3 structural units in the IR spectra with increase in the concentration of the crystallizing agent NiO up to 0.8 mol%, clearly suggests an increasing modifying action of these ions. It may be noted here that it is the octahedral ion that induce more non-bridging oxygens and structural disorder in the glass network. Hence, the analysis of IR spectral studies of the samples points out that there is a gradual transformation of nickel ions from octahedral to tetrahedral positions as the concentration of NiO is increased beyond 0.8 mol%.

The values of dielectric parameters viz., ε', tan δ and σ_{ac} at any frequency are found to increase with temperature and activation energy for a.c conduction is observed to decrease with increase in the content of nucleating agent NiO up to 0.8 mol%; this is an indication of an increase in the space charge polarization. Such increase indicates the increasing concentration of Ni^{2+} ions that act as modifier in these samples. These modifying ions as mentioned earlier, generate bonding defects in the glass network. The defects

thus produced create easy path ways for the migration of charges that would build up space charge polarization and facilitate to an increase in the dielectric parameters as observed [44, 45].

We have obtained the increase in the value of $(\tan\delta)_{max}$ and decrease of the effective activation energy associated with the dipoles with increase in the content of NiO (up to 0.8 mol%) in the glass ceramic network (Table 6), these observations suggest an increasing freedom for dipoles to orient in the field direction, obviously due to increasing degree of disorder in glass ceramic network. The observed dielectric relaxation effects in PbO-Sb_2O_3-As_2O_3 glasses crystallized with different concentrations of NiO may be attributed to the association of octahedrally positioned Ni^{2+} ions with a pair of cationic vacancies as observed in a number of conventional glasses, glass ceramics and crystals that contain divalent positive ions as reported before [46].

The variation of log $\sigma(\omega)$ vs. activation energy for conduction (in the high temperature region) is shown as inset (b) in Fig. 11; the graph yields a near straight line. This observation suggests that the conductivity enhancement is directly related to the thermally stimulated mobility of the charge carriers in the high temperature region. The progressive increase of conductivity with the increase of nickel content in the glass ceramic is a

manifestation of the increasing concentration of mobile electrons, or polarons, involved. The low temperature part of the conductivity (a near temperature independent part, as in the case of present glass ceramics up to nearly 75 ^{o}C) can be explained on the basis of quantum mechanical tunneling model as suggested by Mott [47] with the procedure reported in a number of our earlier papers [48, 49]. Based on quantum mechanical tunneling model, $N(E_F)$ is the density of the energy states near the Fermi level have been evaluated and values obtained are presented in Table 7. The value of $N(E_f)$ obtained $\approx 10^{20}$ eV^{-1} cm^{-3}; such values of $N(E_F)$ suggest the localized states near the Fermi level are responsible for conduction. Further, the value of $N(E_F)$ is found to increase gradually from the sample N_2 to sample N_8, indicating an increase in the degree of disorder in the glass network.

Recollecting once again the observations on optical absorption and magnetic properties, and even dielectric studies reveal that the ratio Ni^{2+} (oct) /Ni^{2+} (tet) increases with increasing concentration of NiO crystallizing agent up to 0.8 mol% in the PbO-Sb_2O_3-As_2O_3 glass ceramics; further, the d–d transitions of the tetrahedral complexes are electric dipole allowed whereas those of octahedral complexes are electric dipole forbidden and are mainly due to the static or dynamic distortions from the regular octahedral geometry of the glass network and they can also be magnetic dipole allowed. As was

reported by a number of other researchers [1], it is the octahedrally positioned Ni^{2+} ion that is responsible for the important luminescence emission transition $^3T_2(F) \rightarrow {}^3A_2(F)$ that peaks around 1280 nm; although we could not record the luminescence emission in the NIR range for lack of facility, the high intensity of octahedral optical absorption bands including $^3A_2(F) \rightarrow {}^3T_2(F)$ and the results of the magnetic moments clearly indicate the possibility of high luminescence emission in glass ceramic sample N_8.

5.6 Conclusions

$40PbO\text{-}(20\text{-}x)Sb_2O_3\text{-}40As_2O_3$ glasses were crystallized with different concentrations (x=0 to 1.5 mol%) of NiO. The XRD, SEM and DTA studies have indicated the presence of different crystalline phases in these samples. The studies on optical absorption and magnetic properties have indicated that there is a higher concentration of nickel ions that occupy tetrahedral positions in the samples crystallized with more than 0.8 mol% of NiO. The dielectric studies have indicated the growing degree of disorder in the glass network with increase in the concentration of crystallizing agent NiO up to 0.8 mol%; from these results it is concluded that within the concentration range of 0.2 to 0.8 mol%, the nickel ions mostly occupy octahedral positions and induce bonding defects causing the enhancement of the values of dielectric parameters. Finally, from the careful analysis of these results, it is

felt that there is a possibility for getting high intense lasing emission (corresponding to $^3A_2(F) \rightarrow {}^3T_2(F)$ transition in the NIR region) if these glasses are crystallized with about 0.8 mol% of NiO.

References

1. B. Wu, N. Jiang, S. Zhou, D. Chen, C. Zhu, J. Qiu, *Opt. Mater.* 30 (2008) 1900.

2. A.M. Malyarevich, Yu.V. Volk, K.V. Yumashev, V.K. Pavlovskii, S.S. zapalov, O.S. Dymshits, A.A. Zhilin, *J. Non-Cryst. Solids* 351 (2005) 3551.

3. M. Srinivasa Reddy, S.V.G.V.A. Prasad, N. Veeraiah, *Phys. Stat. Solidi (a)* 204 (2007) 816.

4. B.V. Raghavaiah, C. Laxmikanth, N. Veeraiah, *Optics Commun.* 235 (2004) 341.

5. P.C. DeRose, M.V. Smith, K.D. Mielenz, D.H. Blackburn, G.W. Kramer, *J. Lumin.* 129 (2009) 349.

6. H. Keppler, N. Bagdassarov, *Chem. Geo.* 158 (1999) 105.

7. E. Zannoni, E. Cavalli, M. Bettinelli, *J. Phys. Chem. Solids* 67 (2006) 789.

8. S. Wang, K. Liang, *J. Non-Cryst. Solids* 354 (2008) 1522.

9. G. Murali Krishna, Y. Gandhi and N. Veeraiah, *Phys. Stat. Solidi (a)* 205 (2008) 177.

10. T. Suzuki, Y. Arai, Y. Ohishi, *J. Lumin.* 128 (2008) 603.

11. A. Jouini, A. Yoshikawa, Y. Guyot , A. Brenier, T. Fukuda, G. Boulon, *Opt. Mater.* 30 (2007) 47.

12. E. Baiocchi, M. Bettinelli, *J. Non-Cryst. Solids* 46 (1981) 203.

13. A. Paul and A.N. Tiwari, *J. Mater. Sci*. 9 (1974) 1057.

14. T. Okokawa, M. Shibata, M. Ookawa, *J. Non-Cryst. Solids* 190 (1995) 226.

15. J.L. Rao, G.L. Narendra and S.V.J. Lakshman, *Polyhedron*, 9 (1990)1475.

16. A. Musinu, G. Piccaluga, P.H. Gaskell, *J. Non-Cryst. Solids* 192 (1995) 32.

17. A. Corrias, A. Musinu and P.H. Gaskell *J. Non-Cryst. Solids* 192 (1995) 49.

18. T.K. Kundu, D.K. Chakravorty, *J. Mater. Res*. 14 (1999) 1069.

19. R.S. Singh, S.P. Singh, *Phys. Chem. Glasses* 40 (1999) 235.

20. I. Kashif, H. Farouk, S.A. Aly J. *Mater.Sci. Mater. Electronics*, 2 (1991) 216.

21. F.A. Khalifa, Z.A. El-hadi, F.M. Ezz, *J. Mater. Sci. Lett*. 10 (1991) 1184.

22. El-Desoky, S.M. Mohamed, I. Kashif, *J. Mater. Sci. Mater. Electronics* 10 (1999) 279.

23. V. Rajendran, F.A Khalifa, H.A. El-Batal, *Ind. J. Pure. Appl. Phys.* 35 (1997) 618.

24. B. Brendeback, R. Glaum, M. Funke, F. Reinauer, J. Hormes and H. Modrow, *Z. Naturforsch* 60a (2005) 449.

25. M. Tawati Daefalla, M.J.B. Adlan, *Ceram. Int*. 30 (2004) 1737.

26. T. Suzuki, G.S. Murugan, Y. Ohishi, *Appl. Phys. Lett*. 86 (2005) 131903.

27. T. Suzuki, Y. Arai and Y. Ohishi, *J. Non-Cryst. Solids* 353 (2007) 36.

28. P. Nageswara Rao, G. Naga Raju, D. Krishna Rao, N. Veeraiah, *J. Lumin.* 117 (2006) 53.

29. H. Schlenz, F. Reinauer, R. Glaum, J. Neuefeind, B. Brendebach and J. Hormes, *J. Non-Cryst. Solids* 351 (2005) 1014.

30. Powder Diffraction File, Alphabetical Index, Inorganic Compounds 2003, Published by JCPDS–International Centre for Diffraction Data, Newtown Square, PA. 19073-3273.

31. A. Bishay, C. Maghrabi, *Phys. Chem. Glasses* 10 (1969) 1.

32. P. Subbalakshmi, P.S. Sastry, N. Veeraiah, *Phys. Chem. Glasses* 42 (2001) 307.

33. B. Dubois, J.J. Videau, J. Portier, *J. Non-Cryst. Solids* 88 (1986) 355.

34. P.J. Miller, C. A. Cody, *Spectrochim. Acta A* 38 (1982) 555.

35. B.V. Raghavaiah, N. Veeraiah, *Phys. Stat. Solidi (a)* 199 (2003) 389.

36. J.J. Kleperis, P.D.Cikmach, A. Lusis, *Phys. Stat. Solidi (a)* 83 (1984) 291.

37. T. Satyanarayana, I.V. Kityk, M. Piasecki, P. Bragiel, M.G. Brik, Y. Gandhi and N. Veeraiah, *J. Phys. Cond. Matt.* 21 (2009) 245104.

38. Y.R. Zakis, A.R. Lusis, Y. Lagzduns, *J. Non-Cryst. Solids* 47 (1982) 267.

39. D. Holland, *Solid State NMR* 26 (2004) 72.

40. A. Marotta, A. Buri, F. Branda, *J. Mater. Sci.* 16 (1981) 341.

41. E. Zamoni, M. Bettinelli, *J. Phys. Chem. Solids* 60 (1999) 449.

42. J.L. Rao, G.L. Narendra, S.V.J. Lakshman, *Polyhedron* 9 (1990) 1475.

43. J.D. Lee, *Concise Inorganic Chemistry,* Fifth Edition, Blackwell Science Ltd., 1996.

44. M. Nagarjuna, T. Satyanarayana, V. Ravi Kumar, N. Veeraiah, Physica *B:Condensed Matter* 404 (2009) 3748.

45. Y. Gandhi, K.S.V. Sudhakar, T. Satyanarayana and N. Veeraiah, *Mater.Chem. Phys.* DOI: 10.1016/j.matchemphys.2009.10.026

46. S.V.G.V.A. Prasad, M. Srinivasa Reddy, N. Veeraiah, *J. Phys. Chem. Solids* 67 (2006) 2478.

47. G. Austin and N.F. Mott, *Adv. Phys.* 18 (1969) 657.

48. K. Sambasiva Rao, M. Srinivasa Reddy, V. Ravi Kumar, N. Veeraiah, *Mater. Chem. Phys.* 111 (2008) 283.

49. P. Venkateswara Rao, T. Satyanarayana, M. Srinivasa Reddy, Y. Gandhi, N. Veeraiah, *Physica B* 403 (2008) 3751